AMERICAN SOCIETY FOR MICROBIOLOGY | Applied and Environmental Microbiology®

ENVIRONMENTAL MICROBIOLOGY

Bacterial Glycogen Provides Short-Term Benefits in Changing Environments

Karthik Sekar,[a] Stephanie M. Linker,[a,b] Jen Nguyen,[c,d] Alix Grünhagen,[a] Roman Stocker,[c] Uwe Sauer[a]

[a]Institute of Molecular Systems Biology, Department of Biology, ETH Zurich, Zurich, Switzerland
[b]Laboratory of Physical Chemistry, Department of Chemistry, ETH Zurich, Zurich, Switzerland
[c]Institute of Environmental Engineering, Department of Civil, Environmental and Geomatic Engineering, ETH Zurich, Zurich, Switzerland
[d]Microbiology Graduate Program, Massachusetts Institute of Technology, Cambridge, Massachusetts, USA

Karthik Sekar and Stephanie M. Linker contributed equally to this article. Author order was determined by decreasing seniority.

ABSTRACT Changing nutritional conditions challenge microbes and shape their evolutionary optimization. Here, we used real-time metabolomics to investigate the role of glycogen in the dynamic physiological adaptation of *Escherichia coli* to fluctuating nutrients following carbon starvation. After the depletion of environmental glucose, we found significant metabolic activity remaining, which was linked to rapid utilization of intracellular glycogen. Glycogen was depleted by 80% within minutes of glucose starvation and was similarly replenished within minutes of glucose availability. These fast time scales of glycogen utilization correspond to the short-term benefits that glycogen provided to cells undergoing various physiological transitions. Cells capable of utilizing glycogen exhibited shorter lag times than glycogen mutants when starved between periods of exposure to different carbon sources. The ability to utilize glycogen was also important for the transition between planktonic and biofilm lifestyles and enabled increased glucose uptake during pulses of limited glucose availability. While wild-type and mutant strains exhibited comparable growth rates in steady environments, mutants deficient in glycogen utilization grew more poorly in environments that fluctuated on minute scales between carbon availability and starvation. Taken together, these results highlight an underappreciated role of glycogen in rapidly providing carbon and energy in changing environments, thereby increasing survival and competition capabilities under fluctuating and nutrient-poor conditions.

IMPORTANCE Nothing is constant in life, and microbes in particular have to adapt to frequent and rapid environmental changes. Here, we used real-time metabolomics and single-cell imaging to demonstrate that the internal storage polymer glycogen plays a crucial role in such dynamic adaptations. Glycogen is depleted within minutes of glucose starvation and similarly is replenished within minutes of glucose availability. Cells capable of utilizing glycogen exhibited shorter lag times than glycogen mutants when starved between periods of exposure to different carbon sources. While wild-type and mutant strains exhibited comparable growth rates in steady environments, mutants deficient in glycogen utilization grew more poorly in environments that fluctuated on minute scales between carbon availability and starvation. These results highlight an underappreciated role of glycogen in rapidly providing carbon and energy in changing environments, thereby increasing survival and competition capabilities under fluctuating and nutrient-poor conditions.

KEYWORDS environmental microbiology, glycogen metabolism, metabolism, metabolomics

Citation Sekar K, Linker SM, Nguyen J, Grünhagen A, Stocker R, Sauer U. 2020. Bacterial glycogen provides short-term benefits in changing environments. Appl Environ Microbiol 86:e00049-20. https://doi.org/10.1128/AEM.00049-20.

Editor Isaac Cann, University of Illinois at Urbana-Champaign

Address correspondence to Uwe Sauer, sauer@imsb.biol.ethz.ch.

Received 9 January 2020
Accepted 26 February 2020
Accepted manuscript posted online 28 February 2020
Published 17 April 2020

Microbes must adapt to, and compete under, changing nutrient conditions. Instead of a well-mixed environment, bacteria in the wild often experience a feast-or-famine existence. Many microbial habitats are characterized by long periods of nutrient starvation, intermittently punctuated by nutrient availability (1). Thus, microorganisms face strong selective pressure to resume growth quickly when nutrients once again become available, and a diversity of strategies has evolved (2, 3). Generally, these strategies involve the accumulation of unused resources that are labile and are quickly activated when richer nutrient environments permit fast growth. For example, *Escherichia coli* facilitates rapid physiological transitions to higher-quality nutrient conditions by maintaining a pool of ribosomes that become translationally active only as available nutrients become more abundant (4–7). *E. coli* also often has additional enzymatic capacity beyond that immediately required (8–10) and accumulates metabolically costly amino acids from protein degradation during starvation; these are rapidly used for RNA and protein synthesis upon the resumption of growth (11). The strategies of other organisms include the accumulation of alanine dehydrogenase in *Bacillus subtilis* to expedite growth after shifts to different environments (12) and the accumulation of methane oxidases, induced by starvation, in the methanotroph *Methyloprofundus sedimenti* in an effort to rapidly convert the next available methane into methanol (13).

Glycogen, a polymer of glucose, is another stored resource common to evolutionarily divergent species. While the role of glycogen as a temporary sugar reserve in mammalian cells is well established, its role in bacteria such as *E. coli* has been less clear. Earlier bacterial studies have linked glycogen with long-term survival, suggesting that it contributes an energy source when the environment does not (14–16), whereas others discuss it as a temporary resource used during the physiological transitions necessitated by dynamic environmental conditions (17–19). Some studies combine the two perspectives, describing a role for glycogen that contributes to survival or maintenance in bacterial environments in which nutrient availability frequently fluctuates (20–22). The concept of glycogen as a nutrient "bank" from which cells withdraw energy, and into which they deposit energy (23), summarizes the prevailing view of the role of glycogen in bacteria; however, it remains to be clarified how long after starvation glycogen continues to supply the cell and toward what physiological processes it is used.

Here, we describe the temporal dynamics of glycogen synthesis and breakdown between periods of nutrient availability and during starvation. Using real-time metabolomics (11) and glycogen measurements, we discovered that glycogen was depleted by >80% within 10 min of entry into starvation conditions and was replenished after 2 min of nutrient availability. By comparing wild-type (WT) cells with cells that are unable to use glycogen, we found that glycogen shortened lag times when cells were switching between carbon sources, enhanced uptake when glucose was limited, and facilitated the transition from a planktonic to a biofilm lifestyle. Importantly, this advantage conferred by glycogen existed only in dynamic or fluctuating environments; glycogen-deficient cells performed comparably to wild-type cells in steady environments. Our results suggest a role for glycogen during physiological transitions that involve starvation. We propose that glycogen serves as a short-term resource, consumed in the minutes after the onset of starvation. The short-term uses of glycogen may lead to long-term benefits, though from our data, it is unlikely that glycogen stores alone directly support bacterial maintenance during extended periods of nutrient starvation.

RESULTS

Cells utilize glycogen upon carbon starvation. In order to investigate the role of glycogen during starvation, we designed a real-time metabolomics experiment to compare the metabolic changes across a transition into starvation of wild-type *E. coli* and a mutant unable to utilize glycogen. Specifically, we harvested mid-log-phase cultures at an optical density at 600 nm (OD_{600}) of 0.8 from minimal medium by fast filtration (24) and resuspended them in the same medium but with a limiting amount of glucose as the sole carbon source (Fig. 1A). We designed the medium in such a way

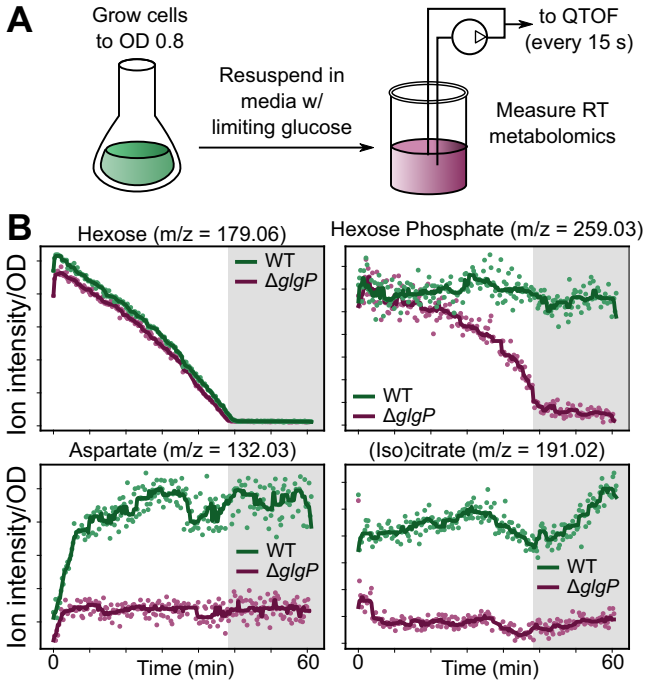

FIG 1 Cells show secondary, glycogen-related metabolic activity upon carbon starvation. (A) Experimental setup for measuring the metabolic profiles of cells with carbon depletion. Growing cells were switched to a medium with limiting glucose (0.32 g/liter); then real-time (RT) metabolomics (11) measurements were carried out for a total of 1 h. For real-time metabolomics measurement, a pump circulated the culture and injected 2 μl of the culture directly into a quantitative time of flight (QTOF) mass spectrometer every 15 s. (B) Glycogen mutant cells exhibit different metabolic activity upon transition to starvation. Shown are traces of exemplary ions that correspond to hexose, hexose phosphate, aspartate, and (iso)citrate for two strains, the wild type (WT) (green) and a *glgP* mutant (purple). Dots represent ion intensity measurements normalized to the initial OD. Shaded areas represent the time period after glucose depletion. Solid lines are a moving average filter of the measured ion intensity.

that the culture would deplete all carbon within 30 to 40 min (see the supplemental material). Across the transition into starvation, we measured more than 100 metabolites as the sum of extra- and intracellular molecules every 15 s using real-time metabolomics (11). In wild-type cells, the ion corresponding to hexoses such as glucose was depleted within 30 to 40 min (Fig. 1B). Several ions annotated to central carbon metabolites diminished immediately after glucose was depleted (see Fig. S1 in the supplemental material), but others, such as hexose phosphate and amino acids, remained stable or even increased, like the tricarboxylic acid (TCA) cycle intermediate (iso)citrate (Fig. 1B). The large number of stable or even increased metabolites suggests ongoing metabolism that is supplied from another source. Given the stable concentration of hexose phosphates and the fact that the first step of glycogen hydrolysis releases glucose-1-phosphate, we hypothesized that glycogen usage may supply metabolism. Indeed, by performing the same experiment with the *glgP* mutant, which is unable to use glycogen, we observed a similar depletion of glucose across the shift into starvation. In contrast to the stable level of hexose phosphates in the wild type, however, they were depleted concurrently with glucose in the *glgP* mutant (Fig. 1B). Additionally, other metabolite levels were lower in the *glgP* mutant than in the wild type (Fig. 1B). Glycogen utilization did not explain the stable levels of all ions during the transition to starvation (Fig. S1B); specifically, the abundances of ions corresponding to the metabolites 3-propylmalate, isopropyl maleate, and orotate remained roughly constant in both strains. Nonetheless, the depletion of hexose phosphates in the *glgP* strain, in contrast to wild-type levels, implicates the utilization of glycogen within minutes of the transition into starvation.

To test the hypothesis that a rapid onset of glycogen breakdown supplies an immediate fuel, we measured cellular glycogen content from the onset of starvation to

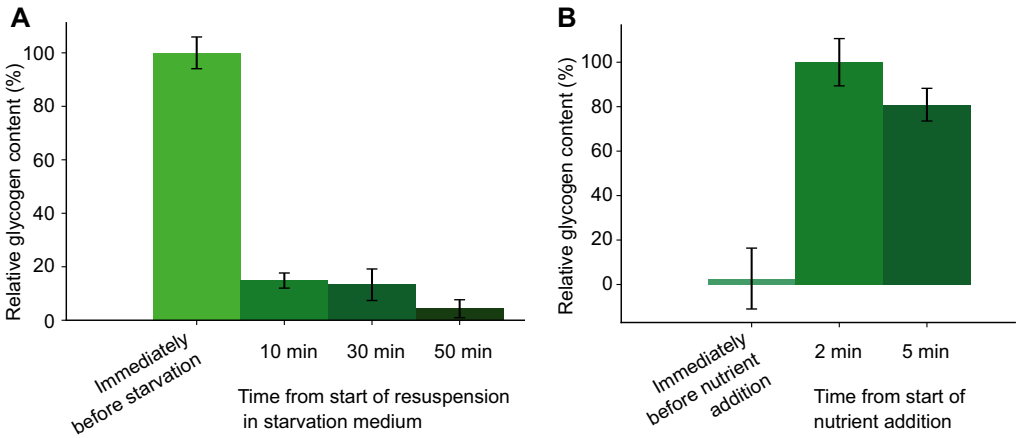

FIG 2 Intracellular glycogen is depleted rapidly after a carbon downshift and accumulates rapidly upon carbon availability. (A) Glycogen depletion during starvation. Wild-type cells were grown to mid-log phase (OD, 0.8) and were resuspended in a medium without carbon. The first sample was taken before resuspension. Error bars indicate the standard errors of six biological replicates. (B) Rapid glycogen synthesis upon the addition of fructose to a carbon-starved culture. Fructose was added at time point zero to wild-type *E. coli* cells harvested at the mid-log phase (OD, 0.8) after 30 min of starvation in a medium without carbon. Error bars indicate the standard errors of three biological replicates.

50 min after starvation (Fig. 2A). We found that glycogen content diminished by 80% within the first 10 min of starvation. Thus, *E. coli* consumes glycogen rapidly after carbon depletion, potentially enabling the pronounced metabolic activity that we observed even hours after entry into starvation (Fig. 1). To elucidate how rapidly the glycogen storage is replenished upon the return of carbon availability, we added fructose to a culture that was carbon starved for 30 min. Fructose was chosen because glucose supplementation would have interfered with the ability to measure glycogen content accurately. Upon fructose addition, the intracellular glycogen content reached a steady level within 2 min (Fig. 2B). Thus, glycogen synthesis and degradation occur on minute time scales, suggesting that glycogen serves a potential role in short-term energy storage in microbes, akin to its role in the mammalian system.

To elucidate the complete dynamics of the metabolic response to glycogen degradation and synthesis, we designed a more-controlled real-time metabolomics experiment. Specifically, after starving a culture for 30 min, we fed glucose at a constant rate of 8 mmol/g (dry weight) of cells/h for 5 min; then we turned off the feed pump, and we measured metabolism for an additional 80 min. The feed rate of 8 mmol/g/h was chosen to be well below the maximum uptake rate of *E. coli* (25, 26), so that glucose would not accumulate abundantly in the medium. In accord with this design, the ion corresponding to glucose was depleted within 1 to 2 min after the feed ceased (see Fig. S2 in the supplemental material). After glucose depletion, we observed sudden drops in the concentrations of all other metabolites, including hexose-6-phosphate, (iso)citrate, and other central carbon metabolites, in both the wild type and the *glgP* mutant (Fig. 3). In contrast to the concentrations in the *glpP* mutant, several metabolites within or near the TCA cycle exhibited a secondary response in the wild type. After initial depletion, isocitrate, in particular, immediately rose again within 5 min to a level near that in the glucose-fed state. This "bounce" effect was also observed prominently in glutamine, glutamate, malate, and aspartate (Fig. 3, green arrows). The fact that the bounce effect was observed primarily in metabolites within or near the TCA cycle (Fig. 3; see also Fig. S3 in the supplemental material) suggests that glycogen is used to fuel respiration right after the onset of starvation.

Overall, we posit that glucose starvation initiates glycogen utilization, both during gradual glucose depletion, as in the earlier experiment, or in the nearly instantaneous depletion here. These observations are consistent with known and suggested interactions of glycogen phosphorylase and glucose uptake-related proteins (18, 27); specifically, the HPr protein involved in glucose uptake positively activates glycogen

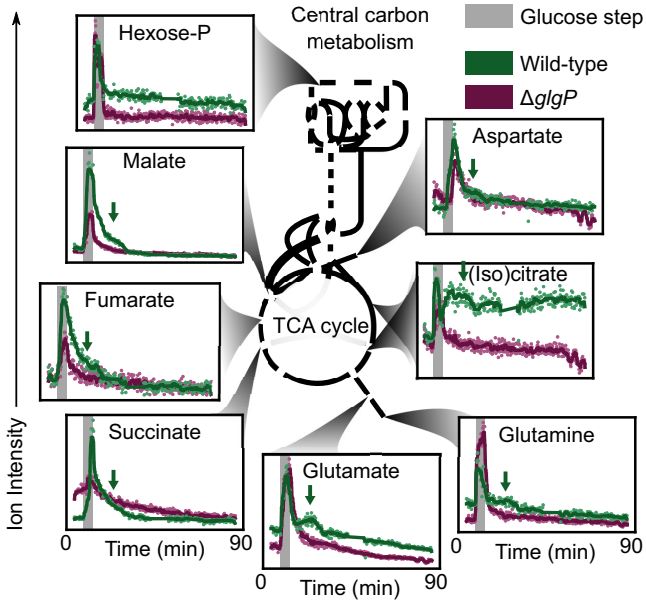

FIG 3 Glycogen-related metabolic response to a brief constant glucose feed. *E. coli* was grown to an OD of 0.8 to 1.2, starved for 30 min without glucose, and then fed a constant glucose supply. The glucose was supplied by a pump at a rate of 8 mmol/g/h to two strains, the wild type (green) and a *glgP* mutant (purple). After 5 min, the glucose feed was stopped. Throughout the feed, real-time metabolomics measurement was performed, and data are shown for ions corresponding to central carbon metabolites. The green arrows indicate a metabolic "bounce," where the measured ion intensity increases within 5 to 15 min for the metabolites malate, fumarate, succinate, glutamate, glutamine, (iso)citrate, and aspartate. Dots indicate ion intensity measurements normalized to the initial OD. Shaded areas indicate the time period when glucose was supplied. Solid lines are a moving average filter of the measured ion intensity.

phosphorylation allosterically. A strongly stimulatory effect occurs when HPr is dephosphorylated, as is typical for starvation. The rapid time scale enabled by allosteric regulation is consistent with our data, which suggest that decreasing glucose uptake rapidly triggers glycogen usage.

Glycogen confers an advantage under changing conditions. The minute scale liquidation of glycogen led us to ask whether glycogen enables cells to accommodate sudden environmental change. To evaluate how glycogen affects the ability to adapt to new environments, we tested two biologically relevant transitions: a change of the nutrient source and the transition from planktonic to biofilm growth. As a control, we first tested the influence of glycogen in stable environments and determined that the difference in the steady-state growth rate between wild-type cells and different glycogen mutants was small (within 15%) (Fig. 4A). Next, we performed a nutrient shift experiment where the wild-type and *glgP* mutant strains were grown to mid-log phase (OD, 0.4) in a glucose medium. After centrifugation and washing, cultures were rapidly transferred to a medium with acetate as the sole carbon source, either directly or after a transitory 30-min period of starvation in a carbon-free medium. Without starvation, the times to resumption of full growth after the switch (i.e., the lag times) were identical for the wild type and the mutant (Fig. 4B). With a period of starvation between the different nutrient sources, however, the glycogen mutant exhibited a lag time roughly double that of the wild type (~220 min versus ~110 min). To test whether this reliance on glycogen was also operative during less-abrupt transitions, we performed a modified lag time experiment, where acetate was added either 60 min before or 60 min after glucose was depleted from the initial medium (Fig. 4C). In agreement with the previous experiment, we found comparable lag times for the glycogen mutant and the wild type without starvation. However, after a period of starvation, the lag time of the glycogen mutant was again significantly longer than that of the wild type. Presumably, the wild type has a shorter lag time after starvation because it either initiates the adaptation

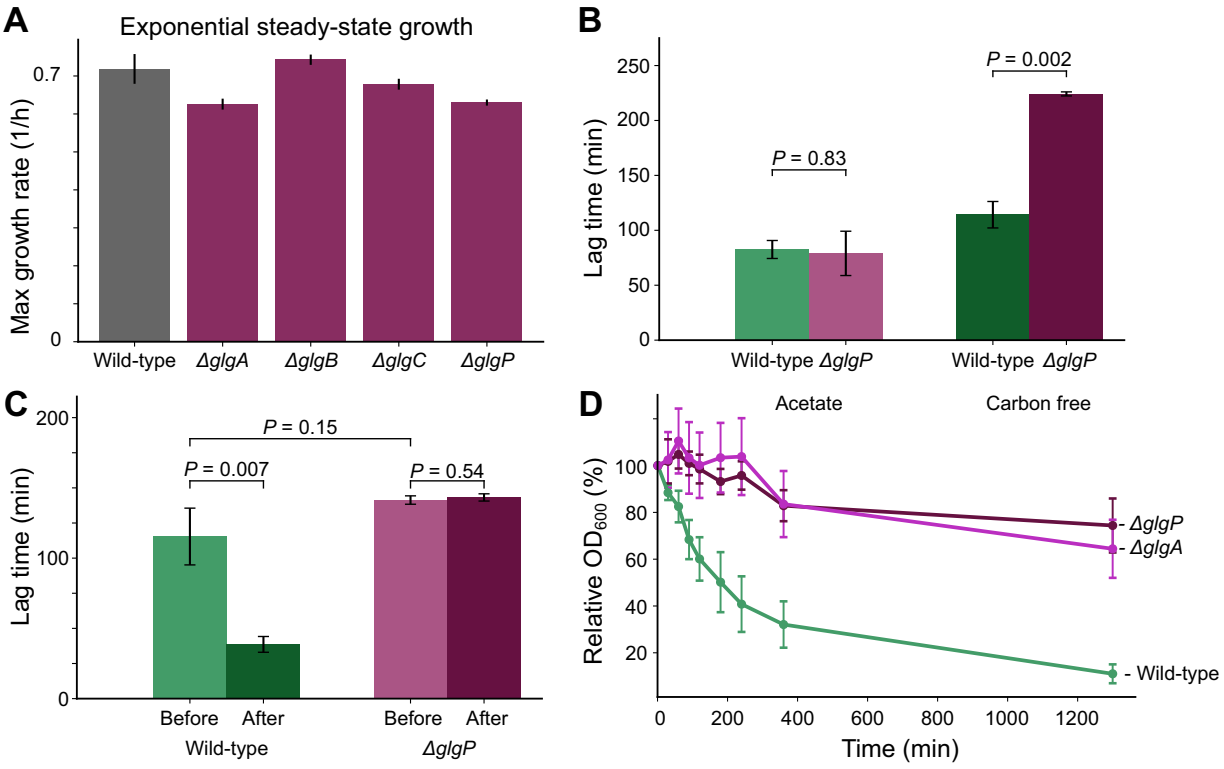

FIG 4 Glycogen-related phenotypes under steady-state versus changing conditions. (A) Glycogen mutants exhibit growth rates similar to that of the wild type during steady-state growth. (B) The *glgP* glycogen mutant exhibits prolonged lag times when starved during a nutrient transition. Wild-type and *glgP* mutant cells were grown to mid-log phase (OD, 0.4) in a glucose medium. Cells were rapidly transferred to an acetate medium either directly or after 30 min of starvation in a carbon-free medium. The lag time until growth resumption was measured for all cells. Error bars indicate the standard errors of three biological replicates, and *P* values were calculated assuming independence with Student's *t* test. (C) Wild-type and *glgP* mutant cells were grown to mid-log phase (OD, 0.4) in a glucose medium. Cells were rapidly transferred to an acetate medium either 60 min before or 60 min after glucose depletion in the initial medium. The lag time until growth resumption was measured for all cells. (D) Glycogen mutants remained planktonic in stationary phase. Wild-type, *glgP* mutant, and *glgA* mutant cells were grown until stationary phase. Afterwards, cells were cultivated without shaking to initiate biofilm formation. Cell attachment was measured via optical density.

before the depletion of the primary carbon source or scavenges previously excreted carbon sources, such as acetate (28–30). Our data suggest that cells that are unable to use glycogen are consequently slower in completing the necessary molecular adaptations for full growth under new conditions. Likely, these cells are deprived of alternative carbon and/or energy sources when experiencing a change in carbon source.

The transition from a planktonic to a sessile (biofilm) lifestyle represents another adaptation that requires substantial restructuring of cellular physiology. Biofilm formation is characterized by three phases: attachment, maturation, and dispersal (31). We focused on the attachment phase, which is characterized by a decrease in the number of planktonic cells. A common method for estimating the concentration of planktonic bacteria relies on measuring the OD_{600}. When stationary-phase *E. coli* was cultured without shaking, the number of planktonic cells decreased by 89% within 18 h (Fig. 4D). The *glgP* and *glgA* mutants, in contrast, remained largely planktonic even after 18 h (with 26% and 36% decreases, respectively). Therefore, wild-type cells have either a higher attachment rate or a higher mortality rate than cells of the glycogen mutant. The latter is unlikely, since our real-time metabolic experiments, which are presented above, have indicated metabolic activity for cells well into starvation. Biofilm formation is induced by nutrient starvation and is inhibited by glucose addition (32, 33). We therefore reason that glycogen facilitates the attachment phase of biofilm formation under starvation conditions, here by providing resources for the production of matrix protein or flagella.

Glycogen utilization confers a growth advantage in dynamic nutrient environments. Given the importance of glycogen during physiological transitions, we sought

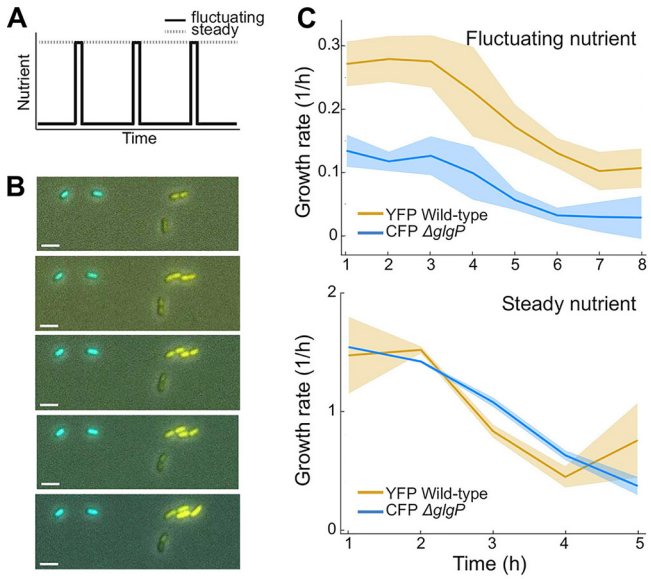

FIG 5 Glycogen consumption offers a growth advantage in pulsing-nutrient environments. (A) Nutrient signals in pulsing and steady environments for microfluidic experiments. The low phases of the fluctuating signal deliver zero carbon for 5 min, while the high phases are 30-s pulses of 2% (vol/vol) LB solution. The steady nutrient maintains a constant concentration of 2% LB solution. (B) Montage of composite images from three channels: phase (gray scale), YFP (yellow), and CFP (cyan). The image frames shown were captured 3 min apart. Bars, 3 μm. (C) Growth rates over time for wild-type and Δ*glgP* populations within pulsing and steady environments. Curves represent the mean growth rates across replicate experiments; error regions (shaded areas) represent standard errors between replicates (three biological replicates across separate days for the pulsing condition; two biological replicates across separate days for the steady condition). In each replicate, at least 1,167 individual *E. coli* cells were observed.

to establish the growth advantage conferred by glycogen utilization under controlled, dynamically changing conditions. By coupling microfluidics and time-lapse imaging, we monitored the volumetric growth of individual *E. coli* cells under conditions of fluctuating or steady nutrient supply. The fluctuating environment consisted of 30-s nutrient pulses followed by 5 min of carbon starvation, whereas in the steady environment, the carbon source was continuously replenished (Fig. 5A). In both environments, precise control over the nutrient signal was maintained by flowing the medium over surface-attached cells and switching between the two media when generating a pulse (26; J. Nguyen, V. Fernandez, S. Pontrelli, U. Sauer, M. Ackermann, and R. Stocker, submitted for publication). In these environments, we competed the yellow fluorescent protein (YFP)-labeled wild-type strain and the cyan fluorescent protein (CFP)-labeled *glgP* mutant, and we monitored their growth through image analysis.

In fluctuating environments, cells capable of consuming glycogen had an apparent growth advantage over those that could not. From time-lapse images, YFP-labeled wild-type cells visibly increased in cell mass and divided often, while the CFP-labeled *glgP* mutant hardly grew in size (Fig. 5B). We then quantified the single-cell growth rate as the rate at which cell volume exponentially doubles, as assessed from image frames captured 3 min apart. In fluctuating environments, these quantifications yielded maximum specific growth rates of 0.28 ± 0.04 h^{-1} and 0.13 ± 0.03 h^{-1} for the wild-type and mutant strains, respectively, whereas in steady environments, the maximum specific growth rates of the two strains were indistinguishable (Fig. 5C). To summarize, the ability to utilize glycogen enhances growth in fluctuating environments, thereby substantiating a key role for glycogen as an immediately available resource across changing environments.

Glycogen utilization enables improved nutrient uptake capability. So far, we have established that glycogen utilization confers a growth advantage in dynamic environments by providing energy and carbon in nutrient-poor transition phases. It is

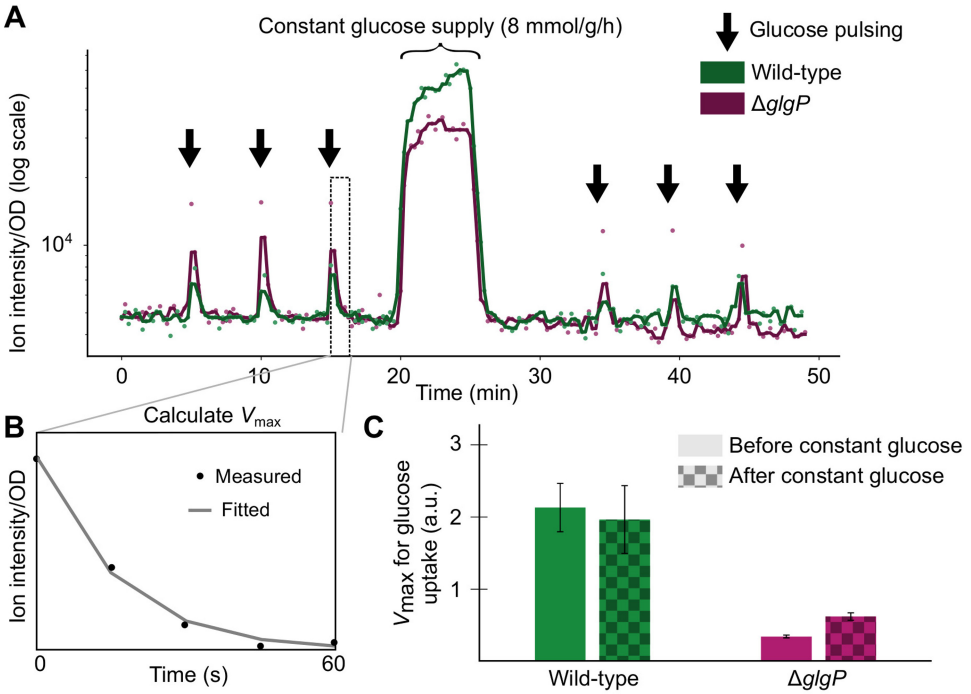

FIG 6 Glycogen capability enables increased scavenging under conditions of starvation. (A) Real-time metabolomics measurement of the ion corresponding to glucose in starved cells. Cells were grown to an OD of 0.8 and were then switched to a medium without carbon. Cellular metabolism was measured with real-time metabolomics as cells were pulse-fed glucose every 5 min, at an integrated feed rate of ~0.4 mmol/g (dry weight) of cells/h (raw data available in the supplemental material). After 20 min, glucose was supplied continuously at 8 mmol/g/h for 5 min. After the constant glucose supply, cells were pulse-fed glucose again every 5 min. Dots indicate the ion intensity measurement normalized to the initial OD. Solid lines are a moving average filter of the measured ion intensity. (B) The kinetics of the glucose uptake were fitted to a Michaelis-Menten equation in order to calculate V_{max} for every pulse. (C) The calculated V_{max} (scavenging ability) is much lower for a *glgP* mutant than for the wild type. The scavenging ability of the *glgP* mutant increases after the constant glucose supply, whereas the scavenging ability of the WT strain is not improved. Error bars indicate the standard errors of the glucose uptake rate for the pulses ($n = 3$).

not clear which cellular functions are supplied by the carbon freed from liquidated glycogen beyond biofilm faculties. Nevertheless, we hypothesized that at least some of the freed carbon would lead to better uptake ability, a paramount survival attribute in scant environments. In order to measure the cellular ability to take up nutrients, we used real-time metabolomics to monitor glucose uptake while switching the cells between periods of starvation and pulses of glucose (26). As in the antecedent study, we observed rapid assimilation of glucose, as indicated by the levels of the ion corresponding to glucose that were detected (Fig. 6A). Each pulse showed an instantaneous increase in the glucose concentration, followed by depletion caused by bacterial consumption. Fitting a Michaelis-Menten model to the glucose consumption, where the uptake rate equals the V_{max} of the fit (Fig. 6B), revealed a much lower maximum capacity for glucose uptake in the *glgP* mutant than in the wild-type (Fig. 6C).

To test whether the difference in uptake capacity stemmed primarily from the carbon release in glycogen, we simulated the carbon release, providing a short dose of carbon by feeding glucose at 8 mmol/g/h for 5 min (Fig. 6A) after the first set of limiting glucose pulses. In agreement with our hypothesis, glucose uptake capacity remained high for the wild type but improved significantly for the *glgP* mutant. Thus, uptake capability does appear to originate from access to a nutrient source during starvation, whether it is internal glycogen or additional carbon input. This carbon supply may fuel the synthesis of uptake-related proteins, which are transcriptionally controlled by starvation-related effectors (e.g., Crp) (34). The carbon supply may also prime the cells metabolically for carbon uptake, for example, through high phosphoenolpyruvate (PEP)

TABLE 1 Strains used in this study

Strain[a]	Genotype
BW25113 (wild type)	Δ(*araD-araB*)*567* Δ(*rhaD-rhaB*)*568* Δ*lacZ4787*(::*rrnB-3*) *hsdR514 rph-1*
Δ*glgP* mutant	Same as BW25113 with Δ*glgP*
Δ*glgA* mutant	Same as BW25113 with Δ*glgA*
Δ*glgB* mutant	Same as BW25113 with Δ*glgB*
Δ*glgC* mutant	Same as BW25113 with Δ*glgC*

[a]For BW25113, see reference 37. For each mutant, the kanamycin marker was excised from the corresponding strain from reference 37.

abundance. PEP is the substrate that phosphorylates incoming glucose through the phosphotransferase system, the primary means of rapid glucose uptake. While we did not measure PEP directly, we noticed differences in the energy charges, AMP and ADP, between the wild type and the glycogen mutant during starvation (Fig. S3 in the supplemental material). Specifically, AMP and ADP were approximately 2.5 and 1.4 times more abundant in the mutant than in the wild type, respectively. Differences in charge are often associated with changes in PEP abundance due to the dependence of PEP-associated carboxylases and kinases on the energy charges (35). In summary, glycogen release enables cells to take up nutrients more rapidly, an important capability when environments change often and nutrients are available only fleetingly.

DISCUSSION

From our findings, we propose a role for bacterial glycogen in dynamic environments. We found that glycogen is used to an appreciable magnitude in a short span of time (~80% within 10 min) as glucose availability falls to zero. This demonstrates that glycogen is not merely a long-term energy storage molecule that supplies microbial maintenance. Instead, glycogen is used within minutes for immediate physiological changes such as the resumption of growth, induction of the attachment phase of biofilm formation, and enabling of nutrient scavenging. Furthermore, glycogen-utilizing cells exhibited higher growth rates in dynamic environments, such as those with single-nutrient shifts or repeated nutrient fluctuations, than glycogen-deficient cells. Taken together, our data reveal glycogen as a crucial internal resource, consumed within minutes of carbon starvation and synthesized within minutes of resumed carbon availability, to aid in the physiological transitions that accompany environmental change.

Environmental change imposes physiological challenges on bacteria. For example, under nutrient-rich conditions, cells are not limited by their ability to scavenge nutrients. However, during starvation, cells must take up diverse nutrients much more efficiently (34, 36). The two scenarios result in a dilemma: the cell has a different objective after switching between carbon-rich and carbon-poor conditions. Meeting the new objective requires an appreciable change either in the abundance of key proteins for uptake or in the metabolic configuration of the cells (e.g., elevated PEP concentrations). Our data depict glycogen as a solution: a fast, flexible store of nutrients. While an inability to use glycogen does not prevent cells from making physiological transitions, the ability to use glycogen seems to increase the rate at which transitions occur. Thus, we show that glycogen is an easy resource for the cell to use to quickly adjust its physiology so as to compete effectively during starvation and under nutrient-poor conditions.

MATERIALS AND METHODS

Strains and plasmids. *E. coli* BW25113 from the Keio collection (37) was used as the wild-type (WT) strain for all experiments. Kanamycin markers were excised from the Keio *glgP*, *glgA*, *glgB*, and *glgC* knockout strains using pCP20, and the gene deletions were verified using PCR (38). All strains used are listed in Table 1, and both plasmids used are listed in Table 2. Strains and plasmids are available on request.

Cultivation, media, and real-time metabolomics profiling. Glucose media and cultures were prepared as described in a previous study (26). On the day before experiments, an inoculum of cells was prepared in sterile Luria-Bertani (LB) broth (10 g/liter NaCl, 10 g/liter Bacto tryptone, and 5 g/liter yeast

TABLE 2 Plasmids used in this study[a]

Plasmid (Addgene ID)	Description
pRSET-B YFP (108856)	Plasmid used to provide constitutive expression of yellow fluorescent protein
pRSET-B CFP (108858)	Plasmid used to provide constitutive expression of cyan fluorescent protein

[a]Both plasmids are from reference 41.

extract) in the morning and was cultivated at 37°C with shaking at 225 rpm until noon. At noon, cells were diluted 1:50 into M9 minimal medium plus 0.4% glucose. In the evening, shake flasks with 35 ml of M9 medium plus 0.4% glucose were prepared with a 1:100 dilution from the M9 inoculum and were cultivated at 30°C with 225 rpm shaking until the next morning. On the morning of the experiment, cells were typically at an OD of 0.1 and were then cultivated at 37°C with shaking at 225 rpm until they reached an OD of 0.8, at which point the experiments were commenced. The M9 minimal medium consisted of the following components (per liter): 7.52 g $Na_2HPO_4{\cdot}2H_2O$, 5 g KH_2PO_4, 1.5 g $(NH_4)_2SO_4$, and 0.5 g NaCl. The following components were sterilized separately and then added (per liter of final medium): 1 ml of 0.1 M $CaCl_2$, 1 ml of 1 M $MgSO_4$, 0.6 ml of 0.1 M $FeCl_3$, 2 ml of 1.4 mM thiamine-HCl, and 10 ml of a trace salt solution. The trace salt solution contained (per liter) 180 mg $ZnSO_4{\cdot}7H_2O$, 120 mg $CuCl_2{\cdot}2H_2O$, 120 mg $MnSO_4{\cdot}H_2O$, and 180 mg $CoCl_2{\cdot}6H_2O$. The real-time metabolomics profiling is fully described in reference 11. Briefly, cells were cultivated in a Schott bottle submerged in a water bath controlled at 37°C. Mixing and aeration were provided by a magnetic stirrer. A peristaltic pump circulated the culture through a six-port valve. On measurement, the valve configuration diverted roughly 2 μl of the culture into a continuous flow of negative ionization buffer (60:40 [vol/vol] isopropanol-water with 1 mM ammonium fluoride [pH 9.0]). The ionization buffer, now mixed with the live cells, was introduced for ionization into an electrospray chamber, and the abundances of the ions were measured semiquantitatively using a quadrupole time of flight (QTOF) mass spectrometry detector (Agilent 6550 system). Measurement (mixing of culture into the buffer) occurred every 15 s, thereby generating a time profile of the intracellular metabolic concentration. The annotation of ions is described in reference 39.

Real-time metabolomics profiling of cells with depleting glucose. Cells were grown to mid-log phase, where the OD_{600} was measured to 0.8. At this point, 32.5 ml of the cells was collected on filter paper using a fast filtration technique (24) and was rapidly resuspended in 25 ml of prewarmed 1:8-diluted M9 medium (37°C), with 0.32 g/liter glucose as the sole carbon source, in a Schott bottle. Immediately after resuspension, the real-time metabolomics profile of the cells was measured for 1 h.

Lag phase experiments. To calculate the lag time of the glucose-to-acetate switch, cells were grown overnight in M9 medium with glucose as the carbon source at 37°C. The next day, cells were freshly inoculated into M9 medium with glucose and were grown to an OD of 0.4. The cells were transferred to M9 medium with acetate either directly or with an intermediate starvation period of 30 min in a carbon-free medium. For the transfer, the collected cells were rapidly filtered, rinsed, and inoculated into 500-ml Erlenmeyer flasks filled with 35 ml of acetate medium. To minimize the stress for the cells, all equipment and solutions were prewarmed to 37°C, and the transfer was performed within $<$2 min. Cell growth was determined by measuring the OD_{600} by spectrophotometry at 0, 15, 45, 90, and 120 min and then every hour up to 420 min after inoculation. The maximal growth rate was calculated using time points after 240 min, and the lag time was calculated as described previously (40).

Biofilm formation. Wild-type, Δ*glgP*, and Δ*glgA* cells were grown overnight at 37°C in LB broth until the cells entered stationary phase. Cells were transferred to a nonshaking environment at room temperature in order to induce biofilm formation. The OD_{600} of the supernatant was measured every ~30 min.

Glycogen content experiments. For the depletion experiment, wild-type cells were grown in M9 medium and glucose to an OD of 0.5 to 0.8. Cells were rapidly transferred to M9 medium without a carbon source to initiate starvation. Samples were taken before starvation and 10 min, 30 min, and 50 min after starvation. For sampling, 1 ml was taken from the culture and was kept on ice. For processing of the samples, they were centrifuged in a cooled centrifuge at maximum speed for 5 min. After centrifugation, 100 μl of the B-PER bacterial protein extraction reagent was added, and the samples were gently shaken for 10 min. The samples were again centrifuged for 5 min at maximum speed in a cooled centrifuge, and the supernatant was transferred to a fresh tube and was stored at −20°C until further processing. For the assay, 25 μl of the supernatant was hydrolyzed and processed as described in the MAK016 assay kit instructions for colorimetric assays (Sigma-Aldrich).

For the replenishment experiment, wild-type cells were grown in M9 medium and glucose to an OD of 0.5 to 0.8. After a starvation period of 30 min in M9 medium without a carbon source, fructose (200 g/liter; an alternative carbon source to minimize signal background with the assay) and thiamine-HCl were added. The samples were taken before the addition of fructose and 2 min, 5 min, and 30 min after the addition and were processed as described above. The glycogen content was measured by a fluorometric method as described in the MAK016 assay kit instructions (Sigma-Aldrich).

Microfluidics setup. The custom method of delivering controlled fluctuating nutrient environments has been described in previous work (Nguyen et al., submitted). In brief, microfluidic channels with a depth of 60 μm were cast in polydimethylsiloxane (PDMS). Each PDMS (Sylgard 184; Dow Corning) device was bonded to a glass slide by plasma treatment of each interacting surface for at least 1 min, and the assembled chip was then incubated for at least 2 h at 80°C. On the morning of each experiment, bonded

channels were cooled to room temperature and were then treated with a 1:10 dilution of poly-L-lysine (catalog no. P8920; Sigma) in Milli-Q water. This treatment enhanced cell attachment but did not affect the growth rate. YFP-labeled wild-type cells and CFP-labeled mutant cells were grown overnight in M9 medium with glucose and ampicillin. The cultures were then inoculated into fresh M9 medium with glucose and ampicillin. After growing to an OD of 0.5 to 1.0, the cells were filtered and transferred to a 1:8-diluted M9 medium without glucose (starvation medium) to a final OD of 0.2. Afterwards, the cells were inoculated into the microchannel. Connecting all inputs and outputs to the microchannel took about 10 to 15 min, allowing ample time for cells to settle and attach to the glass surface within each microchannel before a flow was established. By the onset of the fluctuating nutrient signal, cells had been without carbon for at least 30 min. The fluctuating signal delivered a carbon-free morpholinepropanesulfonic acid (MOPS) medium (Teknova) for 5-min periods, separated by 30-s periods of 2% LB medium (100% LB medium diluted in MOPS medium). The same 2% LB medium was delivered steadily to the nonfluctuating control environment.

Image acquisition and analysis. Bacterial growth within the microfluidic channels was imaged using phase-contrast microscopy with a Nikon Eclipse Ti microscope, equipped with an Andor Zyla sCMOS camera (6.5 μm per pixel) at $\times$60 magnification (40$\times$ objective with 1.5$\times$ amplification), for a final image resolution of 0.1083 μm per pixel. Each position was repeatedly imaged every 3 min. Image series were processed using a custom MATLAB particle-tracking pipeline, which identified individual particles based on pixel intensity and measured particle parameters, such as width and length. These size parameters were used to (i) filter particles that were associated with multiple cells or cells in close proximity to another and (ii) approximate the volume of each single cell as a cylinder with hemispherical caps. The approximated volumes were then used to compute instantaneous single-cell growth rates in terms of volume doublings per hour. Using the equation $V(t + \Delta t) = V(t) \cdot 2^{\mu \Delta t}$ (where V is the volume of a single cell, t is the current time point, Δt is is the change in time between time points, and μ is the growth rate), we calculated μ between each pair of time points, associating the resulting μ with the latter of the two time points.

Data and code availability. All data and code used for figure generation are available at https://github.com/karsekar/glycogen-starvation.

SUPPLEMENTAL MATERIAL

Supplemental material is available online only.

SUPPLEMENTAL FILE 1, PDF file, 0.6 MB.

ACKNOWLEDGMENTS

We thank the members of the Sauer laboratory for useful comments and feedback on the manuscript. We also thank T. Conway for discussions and C. Gao for important advice on the image analysis.

K.S. conceived the project. All authors designed the experiments. K.S., S.M.L., J.N. and A.G. developed the methodology, executed the experiments, and analyzed the data. U.S. and R.S. supervised the work. K.S., S.M.L., and J.N. wrote the manuscript. All authors reviewed and approved the manuscript.

REFERENCES

1. Stocker R. 2012. Marine microbes see a sea of gradients. Science 338:628–633. https://doi.org/10.1126/science.1208929.
2. Bergkessel M, Basta DW, Newman DK. 2016. The physiology of growth arrest: uniting molecular and environmental microbiology. Nat Rev Microbiol 14:549–562. https://doi.org/10.1038/nrmicro.2016.107.
3. Shoemaker WR, Lennon JT. 2018. Evolution with a seed bank: the population genetic consequences of microbial dormancy. Evol Appl 11:60–75. https://doi.org/10.1111/eva.12557.
4. Kohanim YK, Levi D, Jona G, Towbin BD, Bren A, Alon U. 2018. A bacterial growth law out of steady state. Cell Rep 23:2891–2900. https://doi.org/10.1016/j.celrep.2018.05.007.
5. Li SH, Li Z, Park JO, King CG, Rabinowitz JD, Wingreen NS, Gitai Z. 2018. Escherichia coli translation strategies differ across carbon, nitrogen and phosphorus limitation conditions. Nat Microbiol 3:939–947. https://doi.org/10.1038/s41564-018-0199-2.
6. Metzl-Raz E, Kafri M, Yaakov G, Soifer I, Gurvich Y, Barkai N. 2017. Principles of cellular resource allocation revealed by condition-dependent proteome profiling. Elife 6:e28034. https://doi.org/10.7554/eLife.28034.
7. Mori M, Schink S, Erickson DW, Gerland U, Hwa T. 2017. Quantifying the benefit of a proteome reserve in fluctuating environments. Nat Commun 8:1225. https://doi.org/10.1038/s41467-017-01242-8.
8. Davidi D, Milo R. 2017. Lessons on enzyme kinetics from quantitative proteomics. Curr Opin Biotechnol 46:81–89. https://doi.org/10.1016/j.copbio.2017.02.007.
9. O'Brien EJ, Utrilla J, Palsson BO. 2016. Quantification and classification of E. coli proteome utilization and unused protein costs across environments. PLoS Comput Biol 12:e1004998. https://doi.org/10.1371/journal.pcbi.1004998.
10. Sander T, Farke N, Diehl C, Kuntz M, Glatter T, Link H. 2019. Allosteric feedback inhibition enables robust amino acid biosynthesis in E. coli by enforcing enzyme overabundance. Cell Syst 8:66–75.e8. https://doi.org/10.1016/j.cels.2018.12.005.
11. Link H, Fuhrer T, Gerosa L, Zamboni N, Sauer U. 2015. Real-time metabolome profiling of the metabolic switch between starvation and growth. Nat Methods 12:1091–1097. https://doi.org/10.1038/nmeth.3584.
12. Mutlu A, Trauth S, Ziesack M, Nagler K, Bergeest J-P, Rohr K, Becker N, Höfer T, Bischofs IB. 2018. Phenotypic memory in Bacillus subtilis links dormancy entry and exit by a spore quantity-quality tradeoff. Nat Commun 9:69. https://doi.org/10.1038/s41467-017-02477-1.
13. Tavormina PL, Kellermann MY, Antony CP, Tocheva EI, Dalleska NF, Jensen AJ, Valentine DL, Hinrichs K-U, Jensen GJ, Dubilier N, Orphan VJ. 2017. Starvation and recovery in the deep-sea methanotroph Methyloprofundus sedimenti. Mol Microbiol 103:242–252. https://doi.org/10.1111/mmi.13553.
14. Gründel M, Scheunemann R, Lockau W, Zilliges Y. 2012. Impaired glycogen synthesis causes metabolic overflow reactions and affects stress

responses in the cyanobacterium Synechocystis sp. PCC 6803. Microbiology 158:3032–3043. https://doi.org/10.1099/mic.0.062950-0.
15. Wang L, Regina A, Butardo VM, Kosar-Hashemi B, Larroque O, Kahler CM, Wise MJ. 2015. Influence of in situ progressive N-terminal truncation of glycogen branching enzyme in Escherichia coli DH5α on glycogen structure, accumulation, and bacterial viability is still controversial. BMC Microbiol 15:96. https://doi.org/10.1186/s12866-015-0421-9.
16. Wilson WA, Roach PJ, Montero M, Baroja-Fernández E, Muñoz FJ, Eydallin G, Viale AM, Pozueta-Romero J. 2010. Regulation of glycogen metabolism in yeast and bacteria. FEMS Microbiol Rev 34:952–985. https://doi.org/10.1111/j.1574-6976.2010.00220.x.
17. Morin M, Ropers D, Cinquemani E, Portais J-C, Enjalbert B, Cocaign-Bousquet M. 2017. The Csr system regulates Escherichia coli fitness by controlling glycogen accumulation and energy levels. mBio 8:e01628-17. https://doi.org/10.1128/mBio.01628-17.
18. Seok Y-J, Sondej M, Badawi P, Lewis MS, Briggs MC, Jaffe H, Peterkofsky A. 1997. High affinity binding and allosteric regulation of Escherichia coli glycogen phosphorylase by the histidine phosphocarrier protein, HPr. J Biol Chem 272:26511–26521. https://doi.org/10.1074/jbc.272.42.26511.
19. Yamamotoya T, Dose H, Tian Z, Fauré A, Toya Y, Honma M, Igarashi K, Nakahigashi K, Soga T, Mori H, Matsuno H. 2012. Glycogen is the primary source of glucose during the lag phase of E. coli proliferation. Biochim Biophys Acta 1824:1442–1448. https://doi.org/10.1016/j.bbapap.2012.06.010.
20. Bourassa L, Camilli A. 2009. Glycogen contributes to the environmental persistence and transmission of Vibrio cholerae. Mol Microbiol 72:124–138. https://doi.org/10.1111/j.1365-2958.2009.06629.x.
21. Jones SA, Jorgensen M, Chowdhury FZ, Rodgers R, Hartline J, Leatham MP, Struve C, Krogfelt KA, Cohen PS, Conway T. 2008. Glycogen and maltose utilization by Escherichia coli O157:H7 in the mouse intestine. Infect Immun 76:2531–2540. https://doi.org/10.1128/IAI.00096-08.
22. Lee S, Cantarel B, Henrissat B, Gevers D, Birren BW, Huttenhower C, Ko G. 2014. Gene-targeted metagenomic analysis of glucan-branching enzyme gene profiles among human and animal fecal microbiota. ISME J 8:493–503. https://doi.org/10.1038/ismej.2013.167.
23. Bertrand RL. 2019. Lag phase is a dynamic, organized, adaptive, and evolvable period that prepares bacteria for cell division. J Bacteriol 201:e00697-18. https://doi.org/10.1128/JB.00697-18.
24. Rabinowitz JD, Kimball E. 2007. Acidic acetonitrile for cellular metabolome extraction from Escherichia coli. Anal Chem 79:6167–6173. https://doi.org/10.1021/ac070470c.
25. Monk JM, Koza A, Campodonico MA, Machado D, Seoane JM, Palsson BO, Herrgård MJ, Feist AM. 2016. Multi-omics quantification of species variation of Escherichia coli links molecular features with strain phenotypes. Cell Syst 3:238–251.e12. https://doi.org/10.1016/j.cels.2016.08.013.
26. Sekar K, Rusconi R, Sauls JT, Fuhrer T, Noor E, Nguyen J, Fernandez VI, Buffing MF, Berney M, Jun S, Stocker R, Sauer U. 2018. Synthesis and degradation of FtsZ quantitatively predict the first cell division in starved bacteria. Mol Syst Biol 14:e8623. https://doi.org/10.15252/msb.20188623.
27. Tian Z, Fauré A, Mori H, Matsuno H. 2013. Identification of key regulators in glycogen utilization in E. coli based on the simulations from a hybrid functional Petri net model. BMC Syst Biol 7(Suppl 6):S1. https://doi.org/10.1186/1752-0509-7-S6-S1.
28. Mandel MJ, Silhavy TJ. 2005. Starvation for different nutrients in Escherichia coli results in differential modulation of RpoS levels and stability. J Bacteriol 187:434–442. https://doi.org/10.1128/JB.187.2.434-442.2005.
29. Rahman M, Hasan MR, Oba T, Shimizu K. 2006. Effect of rpoS gene knockout on the metabolism of Escherichia coli during exponential growth phase and early stationary phase based on gene expressions, enzyme activities and intracellular metabolite concentrations. Biotechnol Bioeng 94:585–595. https://doi.org/10.1002/bit.20858.
30. Wei B, Shin S, LaPorte D, Wolfe AJ, Romeo T. 2000. Global regulatory mutations in csrA and rpoS cause severe central carbon stress in Escherichia coli in the presence of acetate. J Bacteriol 182:1632–1640. https://doi.org/10.1128/jb.182.6.1632-1640.2000.
31. Weiss N, Obied K, Kalkman J, Lammertink RGH, van Leeuwen TG. 2016. Measurement of biofilm growth and local hydrodynamics using optical coherence tomography. Biomed Opt Express 7:3508–3518. https://doi.org/10.1364/BOE.7.003508.
32. Thomason MK, Fontaine F, De Lay N, Storz G. 2012. A small RNA that regulates motility and biofilm formation in response to changes in nutrient availability in Escherichia coli. Mol Microbiol 84:17–35. https://doi.org/10.1111/j.1365-2958.2012.07965.x.
33. Zhao R, Song Y, Dai Q, Kang Y, Pan J, Zhu L, Zhang L, Wang Y, Shen X. 2017. A starvation-induced regulator, RovM, acts as a switch for planktonic/biofilm state transition in Yersinia pseudotuberculosis. Sci Rep 7:639. https://doi.org/10.1038/s41598-017-00534-9.
34. You C, Okano H, Hui S, Zhang Z, Kim M, Gunderson CW, Wang Y-P, Lenz P, Yan D, Hwa T. 2013. Coordination of bacterial proteome with metabolism by cyclic AMP signalling. Nature 500:301–306. https://doi.org/10.1038/nature12446.
35. Sauer U, Eikmanns BJ. 2005. The PEP–pyruvate–oxaloacetate node as the switch point for carbon flux distribution in bacteria. FEMS Microbiol Rev 29:765–794. https://doi.org/10.1016/j.femsre.2004.11.002.
36. Towbin BD, Korem Y, Bren A, Doron S, Sorek R, Alon U. 2017. Optimality and sub-optimality in a bacterial growth law. Nat Commun 8:14123. https://doi.org/10.1038/ncomms14123.
37. Baba T, Ara T, Hasegawa M, Takai Y, Okumura Y, Baba M, Datsenko KA, Tomita M, Wanner BL, Mori H. 2006. Construction of Escherichia coli K-12 in-frame, single-gene knockout mutants: the Keio collection. Mol Syst Biol 2:2006.0008. https://doi.org/10.1038/msb4100050.
38. Datsenko KA, Wanner BL. 2000. One-step inactivation of chromosomal genes in Escherichia coli K-12 using PCR products. Proc Natl Acad Sci U S A 97:6640–6645. https://doi.org/10.1073/pnas.120163297.
39. Fuhrer T, Heer D, Begemann B, Zamboni N. 2011. High-throughput, accurate mass metabolome profiling of cellular extracts by flow injection-time-of-flight mass spectrometry. Anal Chem 83:7074–7080. https://doi.org/10.1021/ac201267k.
40. Enjalbert B, Cocaign-Bousquet M, Portais J-C, Letisse F. 2015. Acetate exposure determines the diauxic behavior of Escherichia coli during the glucose-acetate transition. J Bacteriol 197:3173–3181. https://doi.org/10.1128/JB.00128-15.
41. Sarabipour S, King C, Hristova K. 2014. Uninduced high-yield bacterial expression of fluorescent proteins. Anal Biochem 449:155–157. https://doi.org/10.1016/j.ab.2013.12.027.